Proc. Natl. Acad. Sci. USA
Vol. 96, pp. 3819–3823, March 1999
Genetics

Pathogenetic sequence for aneurysm revealed in mice underexpressing fibrillin-1

LYGIA PEREIRA*†, SUI YING LEE*, BARBARA GAYRAUD*, KOSTANTINOS ANDRIKOPOULOS*, STEVEN D. SHAPIRO‡, TRACIE BUNTON§, NANCY JENSEN BIERY¶, HARRY C. DIETZ¶‖, LYNN Y. SAKAI**, AND FRANCESCO RAMIREZ*††

*Brookdale Center for Developmental and Molecular Biology, Mount Sinai School of Medicine, One Gustave L. Levy Place, New York, NY 10029; †Istituto de Biociencias, Departamento de Biologia, University of São Paulo, SP 05508 Brazil; ‡Departments of Pediatrics, Medicine, and Cell Biology and Physiology, Washington University School of Medicine at Barnes–Jewish Hospital, St. Louis, MO 63110; §Departments of Comparative Medicine and Pathology and ¶Departments of Pediatrics, Medicine, and Molecular Biology and Genetics, and ‖Howard Hughes Medical Institute, Johns Hopkins University School of Medicine, Baltimore, MD 21205; and **Shriners Hospital for Children, Portland, OR 97201

Communicated by Victor A. McKusick, Johns Hopkins Hospital, Baltimore, MD, January 21, 1999 (received for review October 26, 1998)

ABSTRACT **Dissecting aortic aneurysm is the hallmark of Marfan syndrome (MFS) and the result of mutations in fibrillin-1, the major constituent of elastin-associated extracellular microfibrils. It is yet to be established whether dysfunction of fibrillin-1 perturbs the ability of the elastic vessel wall to sustain hemodynamic stress by disrupting microfibrillar assembly, by impairing the homeostasis of established elastic fibers, or by a combination of both mechanisms. The pathogenic sequence responsible for the mechanical collapse of the elastic lamellae in the aortic wall is also unknown. Targeted mutation of the mouse fibrillin-1 gene has recently suggested that deficiency of fibrillin-1 reduces tissue homeostasis rather than elastic fiber formation. Here we describe another gene-targeting mutation, mgR, which shows that underexpression of fibrillin-1 similarly leads to MFS-like manifestations. Histopathological analysis of mgR/mgR specimens implicates medial calcification, the inflammatory–fibroproliferative response, and inflammation-mediated elastolysis in the natural history of dissecting aneurysm. More generally, the phenotypic severity associated with various combinations of normal and mutant fibrillin-1 alleles suggests a threshold phenomenon for the functional collapse of the vessel wall that is based on the level and the integrity of microfibrils.**

Elastic fibers are extracellular macroaggregates in tissues that are normally subjected to stretching and expansile forces (1). Elastic fibers are made of an elastin core surrounded by microfibrils. Fibrillin-1 is the major structural component of the microfibrils and the defective gene product in the Marfan syndrome (MFS), a dominantly inherited disorder characterized by cardiovascular, skeletal, and ocular abnormalities (2). The cardiovascular manifestations of MFS include aortic root dilation and dissection that result in rupture of the vessel wall and premature death, if left untreated. However, the precise sequence of events underlying aneurysm formation in MFS is ill defined.

The contribution of fibrillin-1 mutations to dissecting aortic aneurysm has been traditionally explained on the basis of histopathological findings in MFS patients and of morphological observations *in vivo* and in cell culture (1, 2). Advanced lesions examined at the time of surgery or death show fragmentation of the elastic fibers with reduced elastin content in the media (2). The appearance of a microfibrillar lattice within and around the core of elastic fibers during embryogenesis suggested a regulatory role of microfibrils in the organized deposition of tropoelastin molecules (1). Fibrillin-1 mutations have been therefore thought to influence negatively microfibrillar assembly, thus preventing normal elastogenesis and ultimately weakening the mechanical properties of the tunica media (3, 4). This popular view was recently challenged by the results of our homologous gene-targeting experiment in the mouse (5).

The strategy for targeting of the mouse fibrillin-1 gene (*Fbn1*) was originally designed to generate an internally deleted molecule by replacing exons 19 to 24 with the neomycin (*neo*) gene under the control of the PGK promoter (5). As predicted, gene targeting gave rise to a mutant allele (also known as mgΔ) that produces internally deleted fibrillin-1 molecules. Additionally, the PGK*neo*-cassette was found to reduce mgΔ expression more than 10-fold. Heterozygous mutant animals appear normal throughout early adult life, conceivably because the relative excess of the wild-type protein overcomes the negative potential of the mgΔ product. By contrast, homozygous mgΔ mice die soon after birth of MFS-like vascular complications but exhibit morphologically normal elastic fibers between focal lesions and in unaffected tissues. Absence of normal fibrillin-1 is compatible with embryonic development and the maturation of seemingly normal elastic matrices. This finding implies that the predominant role of fibrillin-1 is in tissue homeostasis rather than in guiding matrix assembly (5).

Although the mgΔ/mgΔ mice were instrumental in identifying an important function of fibrillin-1, their early demise hampered the characterization of the precise pathogenetic sequence leading to an aortic aneurysm. Moreover, the analysis of a single mouse line did little to elucidate the marked variability in the timing and severity of vascular lesions in the human patient population. The present report describes the characterization of a hypomorphic *Fbn1* mutation (also known as mgR) that implicates the inflammatory–fibroproliferative response in the natural history of dissecting aortic aneurysm. It also suggests that inflammatory macrophages may accelerate this process by stimulating unregulated degradation of the elastic matrix. Finally, the analysis of mice with various combinations of wild-type and mutant *Fbn1* alleles points to a threshold phenomenon for the functional collapse of the vessel wall that is based on the abundance and integrity of microfibrils.

MATERIALS AND METHODS

Production of *Fbn1* Mutant Mice. The engineering of the *Fbn1* targeting vector has been described before (5), and the map of this construct is shown again in Fig. 1. Aside from the

The publication costs of this article were defrayed in part by page charge payment. This article must therefore be hereby marked "*advertisement*" in accordance with 18 U.S.C. §1734 solely to indicate this fact.

PNAS is available online at www.pnas.org.

Abbreviations: MFS, Marfan syndrome; ES, embryonic stem; MMP, matrix metalloproteinase.

††To whom reprint requests should be addressed. e-mail: ramirf01@doc.mssm.edu.

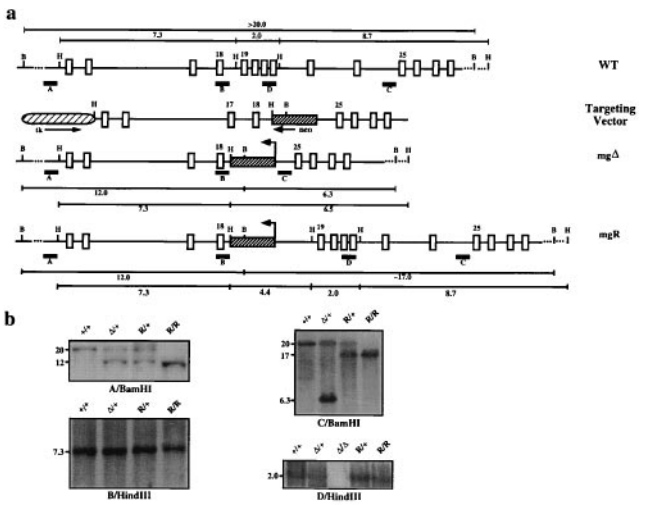

FIG. 1. *Fbn1* gene targeting. (*a*) From top to bottom: the wild-type region that was targeted with the position of the probes (A–D) and the restriction sites used in the Southern analysis; the targeting vector with the arrows indicating the direction of transcription of the selectable marker genes; and the mgΔ and mgR alleles with the *Bam*HI and *Hin*dIII fragments. (*b*) Southern blots of tail DNA from mice with different *Fbn1* genotypes digested with the indicated enzymes and hybridized to the indicated probes. The samples include wild-type (+/+), heterozygous (Δ/+), and homozygous (Δ/Δ) mgΔ mice and heterozygous (R/+) and homozygous (R/R) mgR mice.

Fbn1 sequence, the targeting vector contained the PGK*neo* and PGK*tk* expression cassettes for positive/negative selection of correctly targeted embryonic stem (ES) cells (6). About 60 μg of linearized targeting vector DNA was electroporated into 2×10^7 ES cells of the R1 line (7, 8). The electroporated cells were subsequently selected in the presence of G418 and 1-(2-deoxy-2-fluoro-β-d-arabinofuranosyl)-5-iodouracil (FIAU), and about 200 of the surviving clones were randomly picked and analyzed by *Bam*HI digestion and hybridization to probe A (Fig. 1) (6, 7). Two of the three clones identified as correctly targeted were injected into C57-BL/6 embryos as described (7). Chimeras identified on the basis of agouti pigmentation in the coat were backcrossed and the agouti offspring were genotyped by Southern blot analysis to probe A and B (Fig. 1*a*). Only one of the targeted ES clones was found to have contributed to the germ line of the chimeric mouse. Heterozygous mutant progeny were intercrossed to produce the animals analyzed in this study.

Characterization of the mgR Allele. Southern analyses on the progeny of the intercrosses were performed with probes C and D, in addition to probes A and B (Fig. 1) (9). Long-range PCR amplification was used to clone the regions spanning from the PGK*neo*-cassette to exons 18 and 19 of the targeted mgR allele (10). The resulting products were subcloned into plasmids and multiple independent subclones were sequenced (9). Relative levels of the mgR transcript were estimated by Northern analysis by using total or poly(A)$^+$ RNA purified from skin and lung samples pooled from five newborn animals, and the estimate was based on quantitative scanning of blots using both the NIH IMAGE software and the PhosphorImager analyzer (Molecular Dynamics) (9). Immunoprecipitation of metabolically labeled proteins with pAB9543 polyclonal antibodies against fibrillin-1 was performed on the tissue culture medium of fibroblast lines established from skin explants as previously described (5). Likewise, immunofluorescence analysis of cultured dermal fibroblast was performed as described (5). In the matrix metalloproteinase type 12 (MMP-12) analysis, [^{35}S]-cysteine-labeled fibrillin-1 was immunoprecipitated from the medium of human fibroblast cultures and incubated with 0.1 nM of human recombinant MMP-12 for 20 hr at 37°C (11).

Histological Analysis. Mice were processed as described previously (5). Five-μm sections were stained with hemotoxylin and eosin, and adjacent serial sections were assayed with Verhoeff–van Gieson stain for elastic tissue, trichrome blue stain for collagen, and alizarin red stain for calcium. Immunohistology was performed according to Cartun and Pedersen (12) by using monoclonal antibody F4/80 (Serotec). For skeletal analysis, skin and the majority of soft tissues were removed, and the skeletons were prepared in 95% ethanol for 4 days followed by 2 days in acetone. Cartilage and bone were stained with alcian blue and alizarin red, respectively (13); skeletons were washed and preserved according to Kessel and Gruss (14).

RESULTS

Characterization of the Targeted Allele. The mgR mutation resulted from aberrant targeting by the vector that produced the previously described mgΔ mutant line of mice (5). The mgΔ targeting vector was originally designed to delete six exons of the *Fbn1* gene (5). To this end, the targeting vector DNA was electroporated into both the J1 and R1 lines of ES cells (8). One correctly targeted J1 ES clone and one of the R1-positive ES clones produced chimeric mice that transmitted the *Fbn1* mutation to the next generation. The J1-positive clone produced the mgΔ mouse line, which was reported to exhibit early postnatal lethality when the targeted allele is present in homozygosity (5). By contrast, homozygous mutant mice derived from the R1-positive clone (mgR/mgR) were found to survive significantly longer than mgΔ/mgΔ animals. Southern blot analysis of DNA from mgR/mgR, mgR/+, mgΔ/mgΔ, and wild-type (+/+) animals with four distinct probes revealed that the region 5′ to the PGK*neo*-cassette insertion is identical in the mgΔ and mgR alleles, whereas the region 3′ of it displays restriction patterns consistent with the presence of exon 19 in the mgR allele (Fig. 1*b*). The regions of the mgR allele between the PGK*neo*-cassette and exons 18 and 19 were therefore amplified by long-range PCR and sequenced. This experiment revealed that an unequal crossover had occurred between intron 24 of the targeting vector and intron 18 of the *Fbn1* gene, resulting in the integration of the PGK*neo*-cassette without loss of endogenous sequence (Fig. 1*a*). Consistent with this conclusion, sequencing of reverse transcription—PCR products from mgR/mgR tissues identified only correctly spliced transcripts (data not shown). Interestingly, a 67-bp-long A/T-rich stretch of DNA was found to have been added at the point of transition between introns 24 and 18 in the mgR allele. Additional Southern analyses excluded recombinations resulting from the insertion of the PGK*tk*-cassette or the plasmid sequence (data not shown).

mgR Is a Hypomorphic Mutation. We have previously estimated that insertion of the PGK*neo*-cassette in the mgΔ allele reduces gene expression about 10-fold, probably as a result of transcriptional interference by the strong PGK promoter (5, 15). Because the PGK*neo*-cassette had integrated at about the same position in the mgR allele, we assessed whether gene expression was reduced also in this case. Northern analysis of *Fbn1* mRNA levels in skin samples from +/+, mgΔ/+, and mgR/mgR animals documented ≈5-fold reduction in the expression of the mgR allele (Fig. 2*a*). Identical results were obtained with lung samples (data not shown). Immunoprecipitation of metabolically labeled fibrillin-1 molecules from fibroblasts derived from +/+, mgΔ/mgΔ, and mgR/mgR mice gave a crude indication of the lower expression of the mgΔ compared with the mgR allele and of the latter compared with the wild-type gene (Fig. 2*b*). It additionally showed that the mgR protein is of the same size as wild-type fibrillin-1 and larger than the mgΔ product (Fig. 2*b*). Immu-

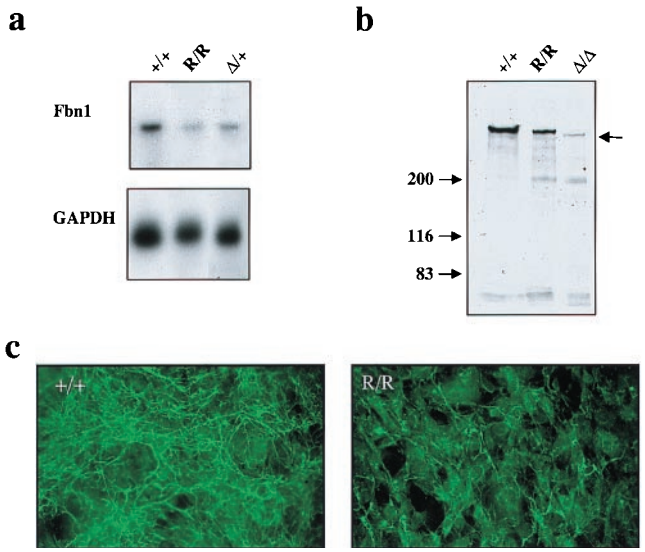

FIG. 2. Characterization of the mgR products. (*a*) Northern blot hybridization of poly(A)$^+$ RNA purified from pooled skin samples hybridized to *Fbn1* and GAPDH probes. The normalized *Fbn1* mRNA expression levels for mgR/mgR and mgΔ/+ tissues, relative to +/+ controls, were 0.28 and 0.52, respectively. (*b*) SDS/PAGE of immunoprecipitated metabolically labeled fibrillin-1 from the medium of cells established from wild-type and mutant animals; arrow points to the fibrillin-1 products. (*c*) Immunofluorescence of cultured dermal fibroblasts from mgR/mgR (R/R) and wild-type (+/+) littermates by fibrillin-1 antisera; cells were processed 72 hr after plating.

nohistochemical comparison of the amount of extracellular fibrillin-1 deposited during 72 hr of culture by mgR/mgR and +/+ fibroblasts genes was also consistent with the lower expression of the mgR allele (Fig. 2*c*). Taken together, these analyses indicated that the mgR allele represents a hypomorphic *Fbn1* mutation.

The mgR Mutation Causes Late-Onset Vascular Disease. Both heterozygous and homozygous mgR mice were born at the expected frequency and showed no phenotypic abnormalities at birth. Unlike mgR/+ mice, homozygous mutant animals developed clinically significant kyphosis and increased dorsal–ventral diameter of the chest because of dramatic overgrowth of the ribs (Fig. 3). Other long bones were at most ≈10% longer than in sex-matched wild-type littermates. Severe kyphosis was generally associated with diaphragmatic hernia. Histologic examination revealed a focal inflammatory infiltrate and muscular atrophy at the ruptured edges (data not shown).

Homozygous mgR mice died naturally at an average age of 3.8 ± 3.4 months. Necropsy was performed on 20 homozygous mutant mice with an age range of <1 wk to 12 mo (Table 1). All but one mouse displayed some form of vascular abnormality. Half of the mice with severe kyphosis exhibited diaphragmatic hernia with thoracic migration of abdominal contents and respiratory distress, suggesting that pulmonary insufficiency may have contributed to death. Others died suddenly in association with hemopericardium, hemothorax, or hemomediastinum, documenting a vascular etiology. Histopathologic examination of sacrificed newborn mice revealed normal vascular anatomy and architecture, including normally formed elastic lamellae in the aortic media. Alizarin red staining of tissues revealed focal linear calcification of intact elastic lamellae as early as 6 wk of age (Fig. 4 *a–c*). Because of the sparsity of lesions, this finding may have gone undetected in younger animals. Calcified segments increased in frequency and coalesced over time in association with clumping of elastic fibers. By 9 wk of age, intimal hyperplasia was evident with sharply demarcated transition zones between normal and

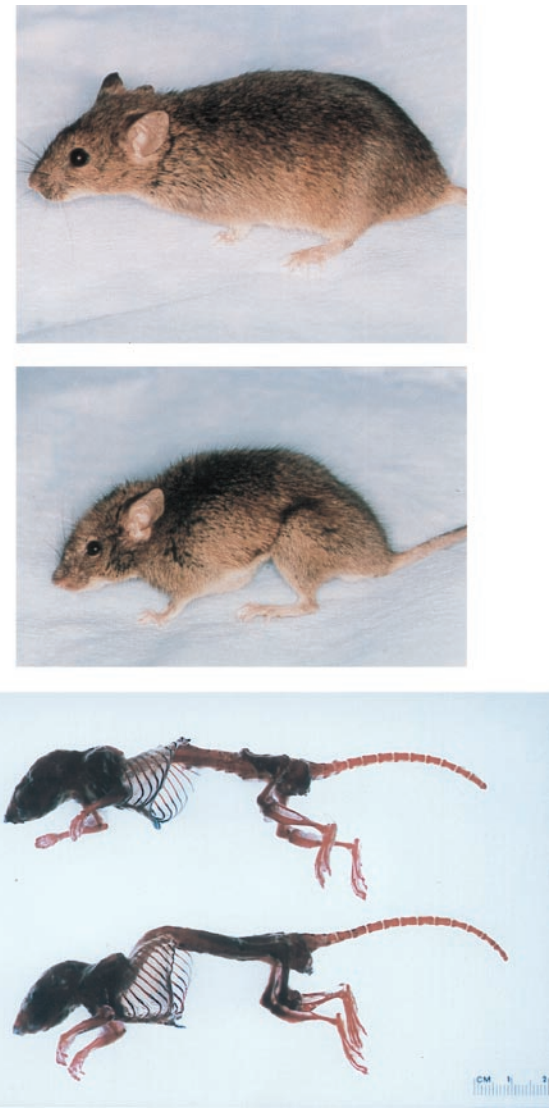

FIG. 3. Clinical presentation of wild-type (*Top*) and homozygous mgR (*Middle*) littermates demonstrating severe kyphosis and overgrowth of the ribs. Alizarin red and alcian blue staining of bone and cartilage, respectively, after removal of soft tissues (*Bottom*).

involved segments (Fig. 4 *d–f*). Intimal hyperplasia generally correlated with the presence of medial calcification. Smooth muscle-cell invasion and hyperplasia were evident within the intima with ectopic, exuberant, and disorganized deposition of collagen and elastin (Fig. 4 *d–f*). Monocytic infiltration of the medial layer, evident from 8 wk on, correlated with fragmentation of elastic lamellae, loss of elastin content, and aneurysmal dilation of the vessel wall. Adventitial inflammation with hyperplasia of fibroblasts was a common finding from 9 wk on.

Secondary Cellular Events Associated with the mgR Mutation. An antibody specific for mature macrophages revealed that only a subpopulation of the inflammatory cells consisted of activated macrophages, but that they tended to cluster at the

Table 1. Clinical findings in mgR/mgR mice

	Total*	Age specified
Medial calcification	8/20	8/16 > 6 wk
Intimal hyperplasia	6/20	6/11 > 9 wk
Medial necrosis and vasculitis	9/20	9/14 > 8 wk
Adventitia hyperplasia with inflammation	12/20	11/16 > 6 wk

*Indicates the fraction of mice examined that displayed the designated findings.

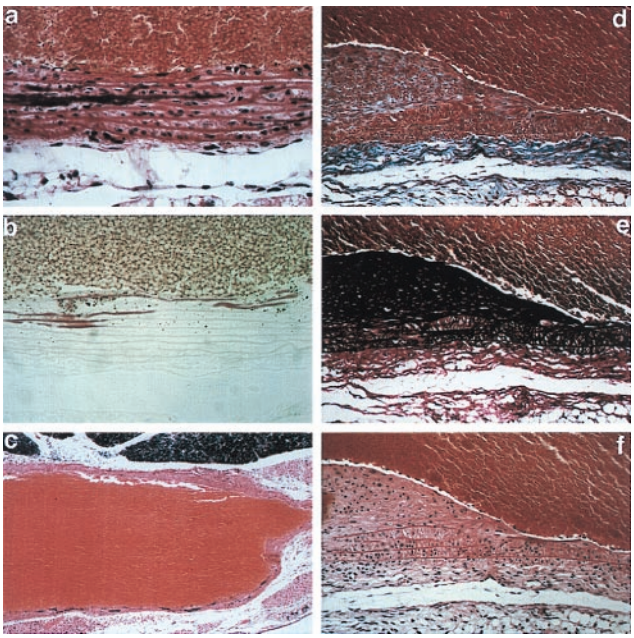

FIG. 4. Histopathology of homozygous mgR mice examined between 6 wk and 3 mo of postnatal life. (*a* and *b*) Calcification of elastic lamellae in the aortic media at 6 wk; staining with hemotoxylin and eosin (*a*) or alizarin red (*b*). (*c*) Aneurysmal dilatation with vessel-wall thinning and calcification of elastic lamellae at 3 mo; hemotoxylin and eosin. (×15) (*d–f*) Intimal hyperplasia with accumulation of excessive collagen and elastin and smooth muscle-cell proliferation and monocyctic infiltration with fragmentation of elastic lamellae in the media at 3 mo. Staining was performed with trichrome blue (*d*), Verhoeff–van Gieson stain (*e*), or hemotoxylin and eosin (*f*). The vessel lumen is at top except in *c*. [×250 *(a, b, d–f)*.]

sites of elastic lamellar fragmentation in early lesions (Fig. 5 *a* and *b*). In the most advanced aneurysms, a tremendous infiltrate of macrophages was found at the adventitial surface with extension into an obliterated tunica media (Fig. 5*c*). In one animal, bony metaplasia with medullary hematopoiesis was seen within the media at the level of the aortic valve annulus (Fig. 5*d*). MMP-12, a macrophage-specific metalloproteinase, is the predominant matrix-degrading proteinase

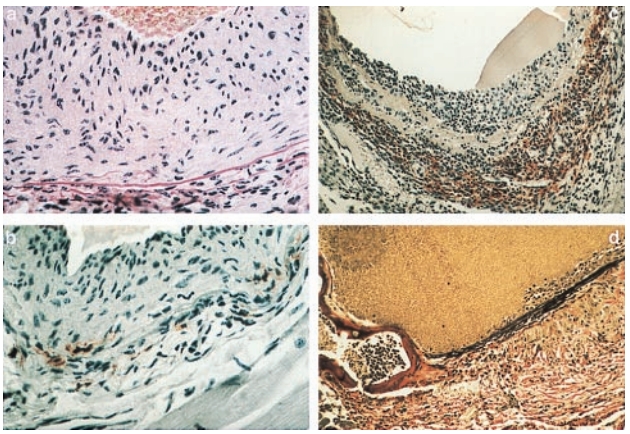

FIG. 5. Histopathology and immunohistochemistry of homozygous mgR mice examined between 3 and 6 mo of postnatal life. (a) Intimal hyperplasia and disorganized elastic lamellae at 3 mo; hemotoxylin and eosin. (*b* and *c*) Horseradish peroxidase immunostaining using mAb F4/80 specific for mature macrophages performed on 3-mo (*b*) and 5–1/2-mo (*c*) specimens. (*c*) Extensive macrophage infiltration at the adventitial border associated with aneurysmal dilatation. (*d*) Bony metaplasia with hematopoiesis within the vessel wall at the junction of the aortic annulus and the ascending aorta at 6 mo; Verhoeff–van Gieson. (×350.)

secreted by mouse macrophages (16). The temporal correlation between inflammatory infiltration and loss of structural integrity of the vessel wall prompted us to examine whether MMP-12 has the capacity to degrade fibrillin-1. Incubation of the recombinant enzyme with fibrillin-1 resulted in the specific cleavage of the protein (Fig. 6). Taken together, these analyses suggest that secondary events initiated by a relative deficiency in fibrillin-1 may include a dynamic and progressive loss of microfibrillar abundance, integrity, and function.

DISCUSSION

The mgR mutation has provided new insights into the function of fibrillin-1-rich microfibrils and MFS pathogenesis. It has also confirmed and extended some of the findings previously made with the mgΔ mutation (5). Homozygous mgR mice produce about a quarter of the normal amount of fibrillin-1 and display phenotypic features in the skeleton and the aorta similar to those of patients with classic MFS. Homozygous mgR mice gradually develop severe kyphosis, probably resulting from loss of tensile strength of the microfibril-rich ligaments and tendons (17). They also exhibit overgrowth of the ribs and, to a much lesser extent, of other long bones. The mechanism responsible for overgrowth in MFS has long been debated. Some researchers have invoked a gain-of-function mechanism of fibrillin-1 mutations in the skeleton, as opposed to a loss-of-function mechanism in the cardiovascular and ocular systems (2). Others have suggested that microfibrils may control bone growth negatively by maintaining periosteal tension and by exerting tensile strength from ligaments and tendons (17, 18). The skeletal findings in the mgR/mgR mice support the notion that microfibrils control bone growth negatively.

The more severe manifestations of the mgR/mgR mice are in the vascular system. Medial calcification was the first pathological sign routinely seen in these animals. Calcification of soft tissues is a poorly understood process that characterizes many pathological conditions. Early biochemical studies have excluded the involvement of a generalized metabolic perturbation in aortic calcification *in vitro* and have instead implicated the extracellular matrix, and particularly the elastic fibers, in the induction of mineral formation (19). Along these lines, more recent gene-targeting work has demonstrated that a ubiquitous matrix component, matrix Gla protein, is a negative regulator of vascular calcification (20). One of the

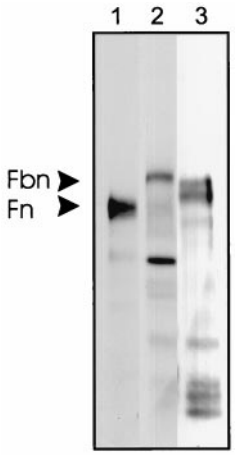

FIG. 6. SDS/PAGE analysis of MMP-12 cleavage of fibrillin-1. Immunoprecipitated metabolically labeled fibrillin was incubated without (lane 2) or with (lane 3) recombinant MMP-12; in lane 1, radioactive fibronectin eluted from gelatin–Sepharose was included as a marker. The ≈200-kDa band seen in lane 2 is an MMP-12-sensitive contaminant of the immunoprecipitation.

mgR/mgR mice also showed striking bony metaplasia. Although inbred C57BL/6J mice have a relatively high incidence of aortic cartilaginous metaplasia, it is unreasonable to conclude that our findings merely manifest this predisposition in the genetic background (21). Calcification was never observed in +/+ and mgR/+ littermates, and mgR/mgR mice were unique in that calcification was not associated with obvious cartilaginous metaplasia, and calcium deposits were confined to elastic lamellar structures. An intriguing explanation for this phenomenon may be based on the following correlative observations: first, cartilaginous metaplasia was also a common finding in rat arteries transduced with an adenoviral vector overexpressing transforming growth factor β (TGFβ) (22); second, binding of the small latent complex of TGFβ to the matrix via latent TGFβ binding protein 1 (LTBP1) has been demonstrated to be required for cytokine activation (23); and third, LTBP1 has been shown to be associated with the microfibrils (24). It is therefore formally possible that reduced fibrillin-1 expression in the aorta may result in more activated TFGβ, and that this may in turn promote cellular proliferation and transdifferentiation of the vascular smooth muscle phenotype (22). A later-stage contributor to vascular disease in mgR/mgR mice is the inflammatory–fibroproliferative response. Macrophages are the major inflammatory cells responsible for matrix degradation. We have presented preliminary and indirect evidence suggesting that inflammation-mediated elastolysis may also participate in the mechanical collapse of the aortic wall. This finding is consistent with the recent finding of altered immunoreactivity for MMPs and tissue inhibitors of MMPs (TIMPs) in vascular specimens from MFS patients (25).

The current model of MFS pathogenesis requires high levels of abnormal fibrillin-1 with dominant—negative, i.e., antimorphic, activity (3, 4). Here we show that fibrillin-1 hypomorphism can also cause MFS. Both antimorphic and hypomorphic mutations have the net effect of reducing microfibrillar abundance. Homozygous mgΔ mice begin life with a drastic reduction in protein and die early because of structural failure of the vascular system (5). Homozygous mgR mice begin life with a relative fibrillin-1 deficiency that is exacerbated by secondary events. Compound mgΔ/mgR heterozygotes die prenatally (data not shown), an outcome consistent with reduced levels of fibrillin-1 and the antimorphic activity of the mgΔ product when paired with nearly equal amounts of normal monomers. Aortic aneurysm and dissection therefore seem to occur once the level and function of microfibrils fall below some critical threshold. This threshold can be present prenatally (mgΔ/mgR), in the neonatal period (mgΔ/mgΔ), or during early adulthood because of secondary events (mgR/mgR). Accumulating evidence indicates that the same secondary events participate in reaching this threshold during late adulthood of mgΔ/+ animals (data not shown). Finally, near-haploinsufficient mice (mgR/+) never reach this threshold and are normal throughout life. It could be further extrapolated that, in contrast to elastin nullizygotes (26), fibrillin-1 null mice would therefore fail to complete embryogenesis. If the pathogenesis of human MFS is comparable to the mgR/mgR scenario, as it may well be with incompletely antimorphic mutations (3, 4), then therapeutic strategies aimed at blocking secondary events may delay or preclude attainment of this critical threshold.

We thank J. Tian and N. Charbonneau for technical assistance and Karen Johnson for preparing the manuscript. This work was supported by National Institutes of Health grants (AR42044, AR41135), Shriners Hospital, Howard Hughes Medical Institute, National Marfan Foundation, Dana and Albert Broccoli Center for Aortic Diseases, Smilow Foundation, and Dr. Amy and James Elster Research Fund.

1. Mecham, R. P. & Davies, E. (1994) in *Extracellular Matrix Assembly and Structure*, eds. Yurchenco, P. D., Birk, D. E. & Mecham, R. P. (Academic, New York), pp. 281–314.
2. Dietz, H., Ramirez, F. & Sakai, L. (1994) in *Advances in Human Genetics,* Vol. 22, eds. Harris, H. & Hirschhorn, K. (Plenum, New York), pp. 153–186.
3. Dietz, H. & Pyeritz, R. (1995) *Hum. Mol. Genet.* **4,** 1799–1809.
4. Ramirez, F. (1996) *Curr. Opin. Genet. Dev.* **6,** 309–315.
5. Pereira, L., Andrikopoulos, K., Tian, J., Lee, S. Y., Keene, D. R., Ono, R., Reinhardt, D. P., Sakai, L.Y., Jensen-Biery, N., Bunton, T., *et al.* (1997) *Nat. Genet.* **17,** 218–222.
6. Li, E., Bestor, T. H. & Jaenisch, R. (1992) *Cell* **69,** 915–926.
7. Andrikopoulos, K., Liu, X., Keene, D. R., Jaenisch, R. & Ramirez, F. (1995) *Nat. Genet.* **9,** 31–36.
8. Nagy, A., Rossant, J., Nagy, R., Abramov-Newerly, W. & Roder, J. C. (1993) *Proc. Natl. Acad. Sci USA* **90,** 8424–8428.
9. Sambrook, E., Fritsch, E. F. & Maniatis, T. (1989) *Molecular Cloning: A Laboratory Manual* (Cold Spring Harbor Lab. Press, Plainview, New York).
10. Dieffenbach, C. W. & Dveksler, G. S. (1989) *PCR Primer: A Laboratory Manual* (Cold Spring Harbor Lab. Press, Plainview, New York).
11. Gronski, T. J., Martin, R., Kobayashi, D. K., Walsh, B. C., Holman, M. C., Van Wart, H. E., Shapiro, S. D. (1997) *J. Biol. Chem.* **272,** 12189–12194.
12. Cartun, R. W. & Pedersen, C. A. (1989) *J. Histotechnol.* **12,** 273–277.
13. McLeod, M. J. (1980) *Teratology* **22,** 299–301.
14. Kessel, M. & Gruss, P. (1991) *Cell* **67,** 89–104.
15. Pham, C. T. N., Mac, D. M., Hug, B. A., Heusel, J. M. & Ley, T. J. (1996) *Proc. Natl. Acad. Sci, USA* **93,** 13090–13095.
16. Shipley, J. M., Wesselschmidt, R. L., Kobayashi, D. K., Ley, T. J., Shapiro, S. D. (1996) *Proc. Natl. Acad. Sci, USA* **93,** 3942–3946.
17. Zhang, H., Hu, W. & Ramirez, R. (1995) *J. Cell Biol.* **123,** 1165–1176.
18. Keene, D. R., Jordan, D., Reinhardt, D. P., Ridway, C. C., Ono, R. N., Corson, G. M., Fairhurst, M., Sussman, M. D., Memoli, V. A. & Sakai, L.Y. (1997) *J. Histochem. Cytochem.* **45,** 1069–1082.
19. Schiffmann, E., Martin, G. R. & Corcoran, B. A. (1964) *Arch. Biochem. Biophys.* **107,** 284–281.
20. Luo, G., Ducy, P., McKee, M. D., Pinero, G. J., Loyer, E., Behringer, R. R. & Karsenty, G. (1997) *Nature (London)* **386,** 78–81.
21. Qiao, J. H., Fishbain, M. C., Demer, L. L. & Lusis, A. J. (1995) *Arterioscler. Thromb. Vasc. Biol.* **15,** 2265–2272.
22. Schulick, A. H., Taylor, A. J., Zuo, W., Qiu, C. B., Dong, G., Woodward, R. N., Agah, R., Roberts, A. B., Vermin, R. & Ditch, D. A. (1998) *Proc. Natl. Acad. Sci. USA* **95,** 6983–6988.
23. Nunes, I., Gleizes, P. E., Metz, C. N. & Rifkin, D. B. (1997) *J. Cell Biol.* **136,** 1151–1163.
24. Taipale, J., Saharinen, J., Hedman, K. & Kaski-Oja, J. (1996) *J. Histochem. Cytochem.* **44,** 875–889.
25. Segura, A. M., Luna, R. E., Horiba, K., Stetler-Stevenson, W. G., McAllister, H. A., Willerson, J. T. & Ferrans, V. J. (1998) *Circulation* **98**II, 331–338.
26. Li, D. Y., Brooke, B., Davis, E. C., Mecham, R. P., Sorensen, L. K., Boak, B. B., Eichwald, E. & Keating, M. T. (1998) *Nature (London)* **393,** 276–280.